scientific reports

OPEN

Computational study of the therapeutic properties of allicin and its nanocomplexes using DFT and molecular docking techniques

E. S. Mozafari[1], Mohammad T. Baei[2]✉ & E. Tazikeh Lemeski[1]

This study investigated the anti-inflammatory, anticancer, antiviral, and antibacterial effects of allicin and its complexes (Allicin/C_{24}, Allicin/$B_{12}N_{12}$, and Allicin/$Al_{12}N_{12}$) using advanced computational techniques such as Density Functional Theory (DFT), Quantum Theory of Atoms in Molecules (QTAIM), and molecular docking. The interactions were analyzed in two phases: gas and aqueous. Results revealed that the Allicin/$Al_{12}N_{12}$ complex exhibited the highest adsorption energy (Ead = -44.43 kcal/mol in the gas phase) and thermodynamic stability (ΔH = -44.36 kcal/mol, ΔG = -29.19 kcal/mol). QTAIM analysis revealed that the Allicin/C_{24} complex involves very weak noncovalent interactions, the Allicin/$B_{12}N_{12}$ complex shows weak covalent bonding with considerable ionic character; and the Allicin/$Al_{12}N_{12}$ complex exhibits stronger covalent interactions with significant electron density sharing. The Allicin/$Al_{12}N_{12}$ complex showed a reduced energy gap (3.44 eV) and higher reactivity than free allicin (5.42 eV). Molecular docking demonstrated that this complex had the strongest binding affinity with biological targets, such as HER2, TNF-α, COVID-19 main protease, and Staphylococcus aureus. UV-Vis and IR spectroscopy revealed significant electronic and vibrational modifications in the complexes, particularly Allicin/$Al_{12}N_{12}$. These findings suggest that nanocages, especially $Al_{12}N_{12}$, can significantly enhance the stability, bioavailability, and therapeutic potential of allicin. The Allicin/$Al_{12}N_{12}$ complex, with its strong binding affinity and favorable electronic properties, has emerged as a promising candidate for treating cancer, inflammation, bacterial infections, and COVID-19. This study highlights the importance of natural products in drug discovery and the role of computational methods in understanding complex biological interactions.

Keywords Allicin, Nanocages, DFT, QTAIM, Molecular Docking, Anti-inflammatory, Anticancer, Antivirus, Antibacterial

Allicin, a bioactive compound derived from garlic (Allium sativum), was first isolated and identified in 1944[1]. The drug has been extensively studied for its wide-ranging pharmacological properties, including anticancer, antibacterial, and anti-inflammatory effects[2]. The therapeutic potential of allicin is mainly due to its unique chemical structure, which allows it to interact with various biological targets and influence key cellular processes. Antibiotic resistance has become an increasingly significant global issue, and the demand for new therapeutic agents is increasing. In this context, allicin has emerged as a promising candidate for drug development[3]. Numerous studies have documented the anticancer properties of allicin, highlighting its ability to induce apoptosis in various cancer cell lines[4]. This effect is achieved by inhibiting cell proliferation and modulating the signaling pathways involved in tumor growth. For example, allicin reduced the expression of oncogenes and increased the expression of tumor suppressor genes. This dual action promotes the death of cancer cells and inhibits their spread. Additionally, allicin's ability to enhance the effectiveness of conventional chemotherapy highlights its potential as a complementary treatment in cancer therapy[5].

In addition to its anticancer properties, allicin has considerable antibacterial activity against a wide range of pathogens, including multidrug-resistant strains[6]. This antimicrobial effect is mainly due to allicin's ability to disrupt bacterial cell membranes and interfere with essential metabolic functions. The increasing incidence of antibiotic resistance calls for alternative antimicrobial agents. Allicin, which has a natural origin and diverse mechanisms of action, is a promising candidate in this search[7]. Allicin's anti-inflammatory properties have

[1]Department of Chemistry, Go.C., Islamic Azad University, Gorgan, Iran. [2]Department of Chemistry, Az.C., Islamic Azad University, Azadshahr, Iran. ✉email: Baei6752@iau.ac.ir; Baei52@yahoo.com

gained significant attention recently. It can help manage chronic inflammatory conditions by modulating inflammatory pathways and reducing the production of pro-inflammatory cytokines[8]. The diverse biological activities associated with allicin make it an important compound in medicinal chemistry.

C_{24}, $B_{12}N_{12}$, and $Al_{12}N_{12}$ nanocages are promising platforms for drug delivery and disease treatment because of their unique structural characteristics and biocompatibility[9]. The C_{24} nanocage, made up of carbon atoms, demonstrates remarkable stability and can encapsulate therapeutic agents. This method facilitates the selective delivery of drugs to specific tissues or cells. This feature is particularly beneficial in cancer therapy because it enables localized drug release, which improves therapeutic effectiveness while reducing systemic side effects[10]. Similarly, $B_{12}N_{12}$ and $Al_{12}N_{12}$ nanocages made from boron nitride and aluminum nitride, respectively, show considerable promise in biomedical applications due to their high surface area and ability to be functionalized[11]. Recent studies indicate that these nanocages can effectively load anticancer drugs like doxorubicin and cisplatin, promoting controlled release profiles that enhance drug bioavailability and mitigate resistance mechanisms in tumor cells[11,12]. Additionally, the natural biocompatibility of $B_{12}N_{12}$ and $Al_{12}N_{12}$ makes them ideal candidates for in vivo applications because they can improve the pharmacokinetics of therapeutic agents[12,13]. Collectively, the integration of C_{24}, $B_{12}N_{12}$, and $Al_{12}N_{12}$ nanocages into drug delivery systems marks a significant advancement for treating various diseases, especially cancer. This approach allows for more efficient and targeted therapeutic strategies. To enhance the therapeutic efficacy of allicin, it is important to explore its combination with these nanocages, specifically the formation of the Allicin/C_{24}, Allicin/$B_{12}N_{12}$, and Allicin/$Al_{12}N_{12}$ complexes. These complexes may show greater stability and bioavailability than free allicin, which could enhance their pharmacological effects. Understanding the interactions between allicin and these nanocages is essential for identifying potential synergistic effects and optimizing therapeutic profiles.

In this study, we utilized advanced computational techniques such as Density Functional Theory (DFT), Quantum Theory of Atoms in Molecules (QTAIM), and molecular docking simulations to investigate the anticancer, antibacterial, and anti-inflammatory effects of allicin and its complexes in both gas and water phases. DFT provides insights into the electronic structure[14,15], adsorption behavior[16–18], optoelectronic properties[19], and stability of various compounds, including those interacting with fullerenes[20,21], fullerene-like cages[22], nanotubes[23–26], and other nanostructures[27], whereas QTAIM offers a detailed examination of their intermolecular interactions and bonding characteristics[16–18]. Molecular docking helps predict the binding affinities between allicin complexes and biological targets, including human epidermal growth factor receptor 2 (HER2), Staphylococcus aureus, COVID-19, and tumor necrosis factor-alpha (TNF-α). This information is valuable for drug design. The choice of biological targets HER2, TNF-α, COVID-19 main protease (Mpro), and Staphylococcus aureus was based on their well-documented roles in cancer progression, inflammation, viral infection, and bacterial pathogenesis, respectively. These targets are closely related to the pharmacological activities of allicin previously reported in the literature. HER2 is a validated oncogenic receptor in breast cancer therapy; TNF-α is a central mediator of inflammation; the COVID-19 Mpro is an essential enzyme for viral replication; and S. aureus represents a clinically relevant pathogen with increasing antibiotic resistance. Docking simulations were performed against these targets to comprehensively assess the multi-target therapeutic potential of allicin and its nano complexes. The primary objective of this research was to conduct a comprehensive computational analysis of the bioactive properties of allicin and its complexes. By integrating theoretical approaches with experimental data, we aim to contribute to the understanding of how these compounds can be harnessed to develop novel therapeutic strategies against cancer and infectious diseases. This work not only highlights the significance of natural products in drug discovery and demonstrates the role of computational methods in elucidating complex biological interactions.

Computational method

This study uses advanced computational techniques to analyze the anticancer, antibacterial, and anti-inflammatory effects of allicin and its complexes: Allicin/C_{24}, Allicin/$B_{12}N_{12}$, and Allicin/$Al_{12}N_{12}$. The methods employed include DFT, Molecular Electrostatic Potential (MEP) analysis, Quantum Molecular Descriptors (QMDs), assessments of solvation energy using the Polarizable Continuum Model (PCM) for water, frequency calculations, evaluations of thermodynamic functions, QTAIM, UV-Vis spectroscopy, and molecular docking simulations.

DFT was used to investigate the electronic structure and stability of allicin and its complexes.

The molecular geometries of these compounds were optimized using the PBE1PBE-D3 method[28], which incorporates Grimme's dispersion correction (GD3BJ)[29], along with an appropriate basis set, such as 6–31 + G**, in Gaussian 09 software (Gaussian 09, Revision A.02)[30], available at https://gaussian.com/g09citation.This level of theory (PBE1PBE-D3/6–31 + G) with D3 dispersion correction has been selected due to its proven reliability in describing non-covalent interactions, including hydrogen bonding and dispersion forces in organic systems[31–35].

After optimization, the adsorption energy (E_{ad}) of the complexes was calculated to assess the stability and potential interactions of allicin with its nanocage complexes using the following equation:

$$E_{ad} = (E_{Allicin/nanocage} + ZPE) - (E_{nanocage} + ZPE) - (E_{Allicin} + ZPE) + E_{BSSE} \quad (1)$$

In this equation, $E_{Allicin/nanocage}$ represents the total energy of the complex formed by allicin and the nanocage after optimization. The term is $E_{nanocage}$ the energy of the nanocage alone, while $E_{Allicin}$ is the energy of the allicin molecule by itself. The zero-point energy (ZPE) is included for each component to ensure accurate comparisons by accounting for quantum mechanical effects. Additionally, E_{BSSE}[36] refers to the basis set superposition error correction, which adjusts for errors that can arise when using finite basis sets in quantum mechanical calculations. To confirm the robustness of the adsorption energy (Ead) calculations, a sensitivity analysis was carried out using a larger basis set (6–311+ +G**). The variations in Ead values were within 1.1 kcal/mol, supporting the reliability of our computational approach.

The MEP maps of allicin and its complexes were calculated, providing valuable insights for predicting reactive sites for electrophilic or nucleophilic attacks. Additionally, the use of QMDs is essential for predicting both molecular reactivity and biological activity because these descriptors are closely related to the structural characteristics of the molecules. The key parameters included in these descriptors are electron affinity (A), ionization potential (I), global softness (S), chemical potential (μ), electronegativity (χ), global hardness (η), and electrophilicity index (ω)[37]. These parameters were derived from density functional theory (DFT) results using the following equations:

$$\mu = -\frac{1}{2}(I + A) \tag{2}$$

$$\chi = -\mu \tag{3}$$

$$\eta = \frac{1}{2}(I - A) \tag{4}$$

$$S = \frac{1}{2\eta} \tag{5}$$

$$\omega = \frac{\mu^{2}}{2\eta} \tag{6}$$

The vibrational modes of allicin and its complexes were analyzed by frequency calculations. This process involved calculating the vibrational frequencies after optimizing the structures to ensure that they represented local minima on the potential energy surface. Additionally, these vibrational frequencies were used to calculate thermodynamic properties, such as changes in enthalpy (ΔH), Gibbs free energy (ΔG), and entropy (ΔS) under standard conditions, using the following equation:

$$\varDelta H = H_{Allicin/nanocage} - H_{nanocage} - H_{Allicin} \tag{7}$$

$$\varDelta G = G_{Allicin/nanocage} - G_{nanocage} - G_{Allicin} \tag{8}$$

$$\varDelta G = \varDelta H - T\varDelta S \tag{9}$$

To analyze the electronic characteristics of allicin and its complexes, we calculated the energy gap (Eg) between the highest occupied molecular orbital (HOMO) and lowest unoccupied molecular orbital (LUMO) using the following equation:

$$E_g = E_{HOMO} - E_{LUMO} \tag{10}$$

QTAIM[38,39] was conducted to analyze intermolecular interactions, identifying hydrogen bonds, van der Waals forces, and other interactions between allicin and its nanocage complexes. A topological analysis of the electron density distributions to characterize bonding interactions.

The solvation energies were calculated using the polarizable continuum model (PCM), which simulates the effects of solvents on allicin and its complexes. Although the SMD model was used to simulate aqueous solvation effects, it may not fully capture explicit solute–solvent interactions at the nanocage interface, such as hydrogen bonding or solvent structuring, which can be significant for polar and reactive systems[40]. Nevertheless, the SMD model was chosen for this study due to its computational efficiency and its proven reliability in capturing bulk solvent effects in a wide range of molecular systems.

Time-dependent DFT (TD-PBE1PBE–D3/6–31 +G**) was used for the UV-visible calculations to obtain excitation energies and corresponding spectra. This approach provides insights into the electronic transitions within the investigated molecules. Molecular docking simulations were conducted to clarify the binding interactions of allicin and its various complexes with multiple biological targets: the HER2 receptor, COVID-19, Staphylococcus aureus bacteria, and TNF-α. The structures of these targets were obtained from protein databases. Using AutoDock 4.2.6 software (AutoDock 4.2.6 and AutoDock Tools)[41], we performed a detailed docking procedure to evaluate the binding affinities and interaction mechanisms between the ligands (allicin and its complexes) and target proteins. The software is available at https://autodock.scripps.edu/download-autodock4.T o validate the docking protocol, redocking simulations were performed by extracting the native ligands from the crystal structures of the target proteins (HER2, TNF-α, COVID-19 Mpro, and Staphylococcus aureus targets) and re-docking them using AutoDock 4.2 under the same grid and docking parameters used for allicin and its complexes. The RMSD values between the co-crystallized and redocked poses were calculated using AutoDock Tools. An RMSD ≤ 2.0 Å was considered acceptable for successful redocking and was used as a criterion for docking reliability[41]. All target proteins demonstrated RMSD values below this threshold, confirming the validity of the docking setup. Also, in the present docking simulations, the receptor molecules were treated as rigid and the ligands (allicin and its complexes) were treated as flexible. This approach, as implemented in AutoDock 4.2[41], is commonly used in preliminary computational screening due to its lower computational cost.

Results and discussion

Optimized structures of allicin and nanocages (C_{24}, $B_{12}N_{12}$, $Al_{12}N_{12}$)

The geometric structures of allicin and three nanocages: C_{24} (fullerene), $B_{12}N_{12}$, and $Al_{12}N_{12}$ were optimized in both gas and aqueous phases using density functional theory (DFT) at the PBE1PBE-D3/6–31 +G** level of theory. The SMD solvation model was used for the aqueous phase calculations. 1 presents the optimized structures along with their corresponding DOS and MEP plots and key bond lengths. Table 1 summarizes the key bond lengths of allicin and the three nanocages for each phase. We did not observe significant differences in the bond lengths of the nanocages between the gas and aqueous phases. However, slight changes in the bond lengths of allicin were noted in the two phases. The C-C, B-N, and Al-N bond lengths in the hexagonal rings of the C_{24}, $B_{12}N_{12}$, and $Al_{12}N_{12}$ nanocages are 1.373, 1.436, and 1.787 Å, respectively. The bond lengths of the square rings were 1.487, 1.481, and 1.852 Å. These results are consistent with those of previous studies[42,43], indicating that our methods are suitable for this study.

DOS analysis provides insights into the electronic structures of allicin and its nanocages. The DOS values of these structures in the gas phase has been calculated and is illustrated in Fig. 1. The energy gaps (Eg) of allicin and the nanocages C_{24}, $B_{12}N_{12}$, and $Al_{12}N_{12}$ are 5.42 eV, 2.78 eV, 7.34 eV, and 4.39 eV, respectively. The corresponding values for the water phase are given in Table 1. These findings agree with previous density functional theory (DFT) calculations[43]. The MEPs of the structures (Fig. 1) visually represent the charge distribution on the molecular surfaces. These maps are valuable for qualitatively determining the presence of electrophilic and nucleophilic sites, with their primary application being the assessment of biological recognition processes[44]. Furthermore, MEP analysis enabled us to identify negative and positive regions of the surfaces, indicated by high (red) and low (blue) electron densities, respectively. In the context of nanocages, the carbon (C), boron (B), and aluminum (Al) atoms are represented as positively charged (blue). In contrast, allicin's oxygen (O) atom of allicin is negatively charged (red). Consequently, the oxygen atom of the allicin molecule was identified as the region most active for interaction with the C, B, and Al nanocages.

Adsorption of allicin on the C_{24}, $B_{12}N_{12}$, and $Al_{12}N_{12}$ nanocages

To assess the potential of C_{24}, $B_{12}N_{12}$, and $Al_{12}N_{12}$ nanocages for use in biological systems and drug delivery, the interaction between allicin and these nanocages was thoroughly investigated. The study employed density functional theory (DFT) at the PBE1PBE-D3/6–31 +G** level to analyze the adsorption process in both gas and aqueous phases. The initial configurations were examined without imposing any geometric restrictions to

Compound	Allicin		C_{24}		Allicin/C_{24}		$B_{12}N_{12}$		Allicin/$B_{12}N_{12}$		$Al_{12}N_{12}$		Allicin/$Al_{12}N_{12}$	
property	Gas	Water	Gas	Water	Gas	Water	Gas	Water	Gas	Water	Gas	Water	Gas	Water
S = O/Å	1.500	1.510	-	-	1.622	1.637	-	-	1.564	1.587	-	-	1.549	1.567
S-S/Å	2.162	2.121	-	-	2.071	2.049	-	-	2.085	2.071	-	-	2.191	2.083
C-C	-	-	1.373	1.373	1.491	1.502	-	-	-	-	-	-	-	-
C-C	-	-	1.487	1.487	1.555	1.557	-	-	-	-	-	-	-	-
B-N	-	-	-	-	-	-	1.436	1.436	1.569	1.575	-	-	-	-
B-N	-	-	-	-	-	-	1.481	1.481	1.572	1.580	-	-	-	-
Al-N	-	-	-	-	-	-	-	-	-	-	1.787	1.789	1.873	1.899
Al-N	-	-	-	-	-	-	-	-	-	-	1.852	1.854	1.910	1.910
D/Å	-	-	-	-	1.487	1.464	-	-	1.549	1.516	-	-	1.925	1.870
E_{ad} (Kcal/mol)	-	-	-	-	−4.78	−10.54	-	-	−31.74	−33.28	-	-	−44.43	−40.28
E_{sol} (Kcal/mol)	-	-	-	-	-	−5.76	-	-	-	−1.54	-	-	-	4.15
ΔH (Kcal/mol)	-	-	-	-	−4.76	−10.61	-	-	−31.62	−33.13	-	-	−44.36	−40.02
ΔG (Kcal/mol)	-	-	-	-	9.12	3.43	-	-	−17.61	−20.13	-	-	−29.19	−27.33
ΔS (cal mol^{-1} k^{-1})	-	-	-	-	−46.56	−47.08	-	-	−46.98	−43.59	-	-	−50.90	−42.57
DM (Debye)	2.42	4.62	0.00	0.00	12.84	20.13	0.00	0.00	10.04	14.86	0.00	0.00	9.82	12.47
E_{HOMO}	−6.73	−7.13	−6.49	−6.36	−5.08	−5.40	−8.31	−8.27	−7.18	−7.52	−6.87	−6.95	−6.18	−6.57
E_{LUMO}	−1.31	−1.35	−3.71	−3.59	−2.92	−3.01	−0.97	−0.87	−2.27	−1.79	−2.48	−2.39	−2.74	−2.16
E_g	5.42	5.78	2.78	2.77	2.16	2.39	7.34	7.40	4.91	5.73	4.39	4.56	3.44	4.41
ΔE_g(%)	-	-	-	-	22.33	13.72	-	-	33.11	22.57	-	-	21.64	3.29
μ	−4.02	−4.24	−5.10	−4.98	−4.00	−4.21	−4.64	−4.57	−4.73	−4.66	−4.68	−4.67	−4.46	−4.37
η	2.71	2.89	1.39	1.39	1.08	1.20	3.67	3.70	2.46	2.87	2.20	2.28	1.72	2.21
χ	4.02	4.24	5.10	4.98	4.00	4.21	4.64	4.57	4.73	4.66	4.68	4.67	4.46	4.37
S	0.18	0.17	0.36	0.36	0.46	0.42	0.14	0.14	0.20	0.17	0.23	0.22	0.29	0.23
ω	2.98	3.11	9.36	8.94	7.41	7.40	2.93	2.82	4.55	3.78	4.98	4.78	5.78	4.32

Table 1. Bond lengths, equilibrium distance (D), adsorption energy (Ead), solvation energy (Esol), enthalpy change (ΔH), Gibbs free energy change (ΔG), entropy change (ΔS), dipole moment (DM), HOMO and LUMO energy values, energy gap (Eg), change of energy gap (Δeg), and quantum molecular descriptors for allicin, C_{24}, $B_{12}N_{12}$, $Al_{12}N_{12}$, Allicin/C_{24}, allicin/$b_{12}n_{12}$, and allicin/$al_{12}n_{12}$ in gas and aqueous phases.

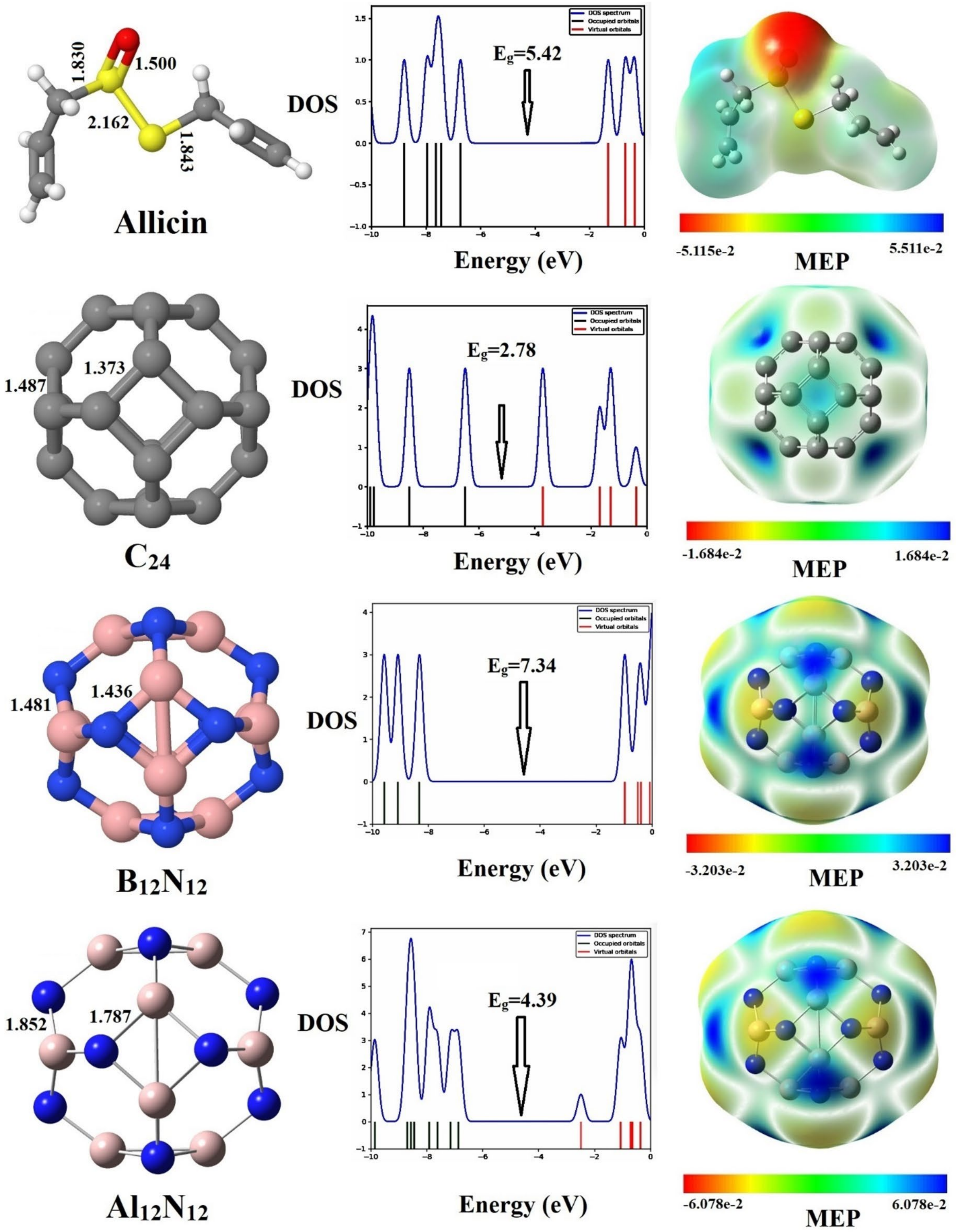

Fig. 1. Optimized structures, DOS, and MEP plots for the allicin molecule, along with C_{24}, $B_{12}N_{12}$, and $Al_{12}N_{12}$ nanocages in the gas phase.

ensure a comprehensive exploration of the adsorption behavior. The most energetically stable configuration for each complex (Allicin/C_{24}, Allicin/$B_{12}N_{12}$, and Allicin/$Al_{12}N_{12}$) was identified based on the lowest total energy obtained after full geometry optimization. This selection was further validated using adsorption energy (Ead) and Gibbs free energy (ΔG) values, where more negative values confirmed the thermodynamic favorability of the chosen configuration. Key parameters, such as bond length, adsorption energy (Ead), thermodynamic properties (ΔH, ΔG, ΔS), solvation energy (Esol), and dipole moments (DM), were calculated to provide a detailed understanding of the interactions and stability of these complexes. The findings are presented in Table 1. Figure 2 shows the optimized geometries, DOS, and MEP maps of the allicin-nanocage complexes. Table 1 summarizes the bond lengths of S = O and S-S in allicin, as well as the C-C, B-B, and Al-Al bonds in the nanocages. Upon the adsorption of allicin onto the C_{24}, $B_{12}N_{12}$, and $Al_{12}N_{12}$ nanocages, significant alterations in these bond lengths were observed. Specifically, the bond lengths of S = O and S-S in allicin, along with the respective bonds in the nanocages (C-C, B-B, and Al-Al), were affected by the interaction. The bond lengths in

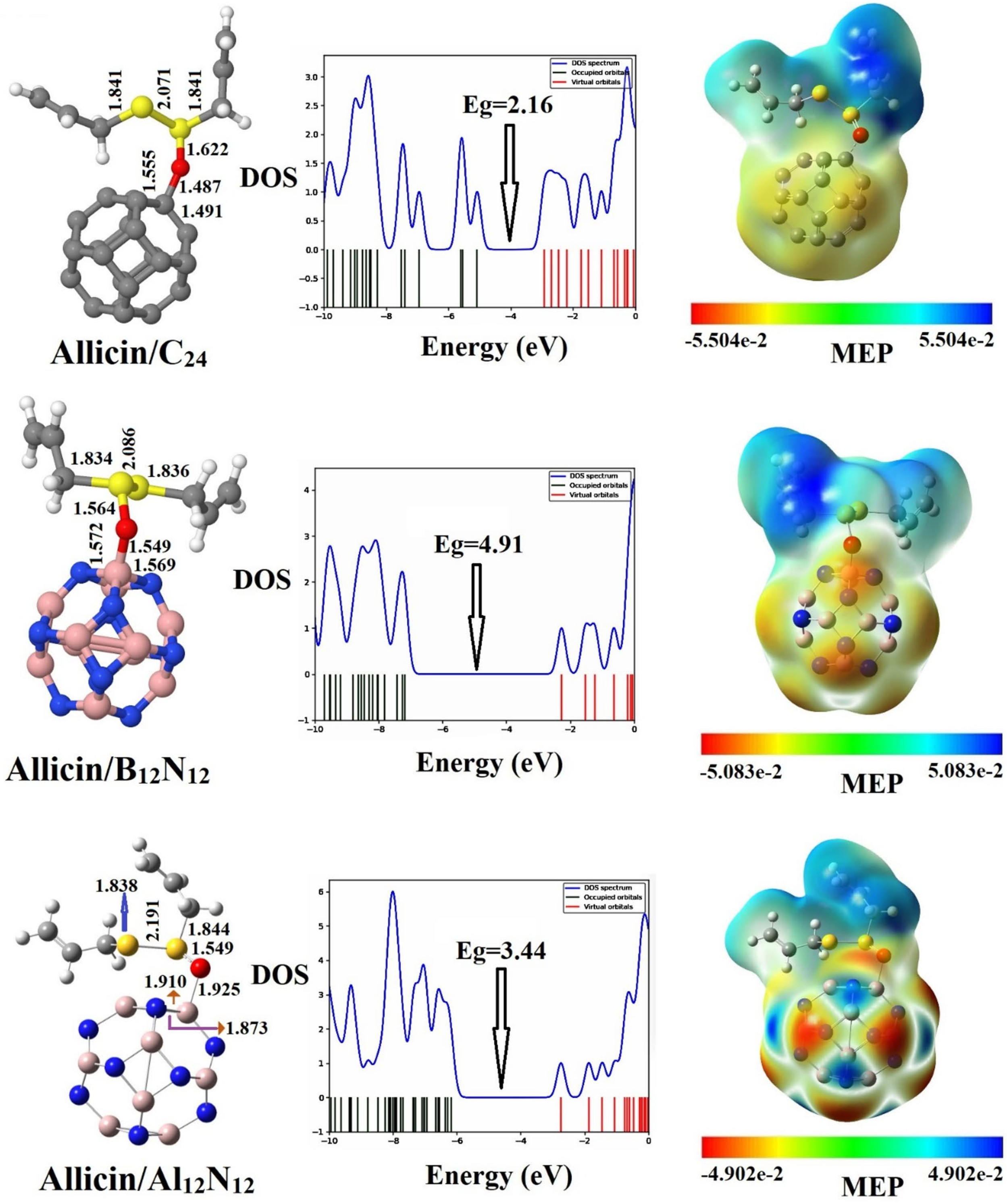

Fig. 2. Optimized structures, DOS, and MEP plots of Allicin/C_{24}, Allicin/$B_{12}N_{12}$, and Allicin/$Al_{12}N_{12}$ complexes in the gas phase.

the nanocages surrounding the interaction sites increased from their initial values. These changes reflect the dynamic nature of molecular interactions and provide valuable insights into the effectiveness of these nanocages for drug delivery[45].

The adsorption energies (Ead) provide critical insights into the thermodynamic favorability of the adsorption process. These values were negative for all three nanocages in both phases, confirming the spontaneous and exothermic interactions. The C_{24} nanocage exhibited adsorption energies of −4.78 kcal/mol in the gas phase and − 10.54 kcal/mol in the aqueous phase, indicating moderate interaction strength. In contrast, the $B_{12}N_{12}$ nanocage showed stronger adsorption, with Ead values of −31.74 kcal/mol in the gas phase and − 33.28 kcal/mol in the aqueous phase. The $Al_{12}N_{12}$ nanocage demonstrated the highest adsorption energies, with values of −44.43 kcal/mol in the gas phase and − 40.28 kcal/mol in the aqueous phase, highlighting its exceptional interaction strength even in aqueous environments. The thermodynamic parameters (ΔH, ΔG, ΔS) of the nanocages were calculated to evaluate the energy changes associated with the adsorption process. All systems exhibited exothermic behavior ($\Delta H < 0$), indicating exothermic adsorption. For the C_{24} nanocage, ΔH was − 4.76 kcal/mol, and ΔG was 9.12 kcal/mol in the gas phase, suggesting less favorable adsorption than the other nanocages. The $B_{12}N_{12}$ nanocage displayed ΔH and ΔG values of 31.62 and 17.61 kcal/mol, respectively, in the gas phase, indicating significant spontaneity. The $Al_{12}N_{12}$ nanocage exhibited the most favorable thermodynamic profile, with ΔH and ΔG values of 44.36 and 29.19 kcal/mol, respectively, in the gas phase. The negative entropy changes (ΔS) for all nanocages suggest a reduction in disorder as allicin binds to the nanocage surfaces. In other words, the systems became more ordered after allicin adsorption than before. The above results revealed that allicin adsorption was thermodynamically more favorable in $Al_{12}N_{12}$ and $B_{12}N_{12}$ nanocages compared to C_{24}.

Solvation energy (Esol) analysis revealed distinct behaviors of the nanocages in aqueous environments. While $Al_{12}N_{12}$ exhibited positive solvation energy (+ 4.15 kcal/mol), its strong intrinsic adsorption energy and significant dipole moment changes counteract this limitation, enhancing its overall suitability for biological applications. In contrast, the C_{24} nanocage had a solvation energy of −5.76 kcal/mol, indicating improved stability in water, while the $B_{12}N_{12}$ nanocage showed a solvation energy of −1.54 kcal/mol, suggesting effective solvation and interaction with biological media. The dipole moments (DM) increased significantly for all complexes after adsorption, improving their solubility and interaction potential in biological environments. The dipole moment of the C_{24} nanocage increased to 12.84 D in the aqueous phase, while that of the $B_{12}N_{12}$ nanocage reached 14.86 D. The $Al_{12}N_{12}$ nanocage demonstrated a dipole moment of 12.47 D in the aqueous phase, indicating enhanced polarity and interaction potential.

Based on the above results, the adsorption of allicin in the C_{24}, $B_{12}N_{12}$, and $Al_{12}N_{12}$ nanocages was thermodynamically favorable in both gas and aqueous phases. While $Al_{12}N_{12}$ exhibited positive solvation energy, strong adsorption energy, enhanced dipole moment, and robust interactions, highlighting its compatibility with drug delivery systems. These findings support the potential of all three nanocages as efficient carriers for biological and pharmaceutical applications, with $Al_{12}N_{12}$ demonstrating the strongest overall performance.

Electronic properties of allicin-nanocage complexes

The electronic properties of allicin and its complexes with nanocages (C_{24}, $B_{12}N_{12}$, and $Al_{12}N_{12}$) were analyzed using density of states (DOS), molecular electrostatic potential (MEP) maps, frontier molecular orbitals (HOMO-LUMO), band gap analysis (Eg), and quantum molecular descriptors (QMDs), as summarized in Table 1. The pristine nanocages exhibited distinct band gaps, with C_{24} showing a moderate value of 2.78 eV, $B_{12}N_{12}$ a high value of 7.34 eV, and $Al_{12}N_{12}$ an intermediate gap of 4.39 eV in the gas phase. Upon allicin adsorption, all complexes exhibited notable reductions in bandgaps, reflecting enhanced electron transport properties. In the gas phase, the Allicin/C_{24} complex showed a 22.33% reduction in the band gap (Eg = 2.16 eV), whereas the Allicin/$B_{12}N_{12}$ complex exhibited the largest reduction (33.11%, decreasing to 4.91 eV. For Allicin/$Al_{12}N_{12}$, the gap was reduced to 3.44 eV (21.64%). These reductions correspond to the introduction of new electronic states near the Fermi level, as revealed by the DOS plots (see Fig. 2). In aqueous conditions, the reduction in bandgaps was less pronounced because of the solvation effects. For instance, the Allicin/$Al_{12}N_{12}$ complex exhibited only a 3.29% reduction in Eg, indicating that water stabilized the electronic structure and moderated the interaction strength.

The MEP maps provided insights into the charge distribution and reactive sites. For free allicin, the oxygen atom in the S= O group exhibited a highly negative potential, making it the most active site for adsorption. After interaction with the nanocages, significant charge redistribution occurred, particularly in the $B_{12}N_{12}$ and $Al_{12}N_{12}$ complexes, which displayed the strongest polarization effects. This redistribution highlights the strong chemisorption of Allicin/$B_{12}N_{12}$ and Allicin/$Al_{12}N_{12}$, aligning with their high adsorption energies in the gas phase. Conversely, the C_{24} complex showed weaker polarization but significant interaction, as indicated by its MEP plot in Fig. 2.

The adsorption of allicin altered the HOMO and LUMO energy levels of the nanocages, facilitating charge transfer. For the Allicin/C_{24} complex, the HOMO level shifted from − 6.49 eV (pristine C_{24}) to −5.08 eV, indicating enhanced electron-donating capability. Similarly, in the Allicin/$B_{12}N_{12}$ complex, significant shifts in the LUMO level resulted in new charge transport pathways, which contributed to the observed band gap reductions. For the Allicin/$Al_{12}N_{12}$ complex, moderate shifts in both the HOMO and LUMO levels were observed, consistent with its intermediate band gap reduction. These changes suggest varying degrees of electronic coupling, with $B_{12}N_{12}$ and $Al_{12}N_{12}$ showing the strongest interactions.

The adsorption of allicin onto the nanocages significantly altered their QMDs, including the chemical potential (μ), global hardness (η), and softness (S), reflecting changes in stability and reactivity. In the gas phase, the chemical potential of the $B_{12}N_{12}$ complex became slightly more negative (from − 4.64 eV to −4.73 eV), suggesting increased stability upon adsorption. For C_{24} and $Al_{12}N_{12}$, μ became less negative (changing from − 5.10 eV to −4.00 eV for C_{24} and from − 4.68 eV to −4.46 eV for $Al_{12}N_{12}$), indicating slightly reduced stability.

A similar trend was observed in the aqueous phase, where only $B_{12}N_{12}$ showed a more negative μ. The global hardness (η) consistently decreased for all complexes after allicin adsorption, reflecting reduced resistance to electronic deformation and enhanced reactivity. For example, in the gas phase, η decreased from 1.39 eV to 1.08 eV for C_{24}, from 3.67 eV to 2.46 eV for $B_{12}N_{12}$, and from 2.20 eV to 1.72 eV for $Al_{12}N_{12}$. Softness (S), the reciprocal of hardness, correspondingly increased, further highlighting the improved reactivity. Similar trends were observed in the aqueous phase.

In summary, the electronic properties of all three complexes were significantly modified upon allicin adsorption, enhancing their potential for drug delivery and biological applications. While the $B_{12}N_{12}$ complex exhibited the most favorable QMD changes, the Allicin/C_{24} and Allicin/$Al_{12}N_{12}$ complexes also showed significant electronic and chemical improvements. These results suggest that the three nanocages, with their unique electronic properties and enhanced reactivity, are suitable candidates for drug delivery and other biological applications.

QTAIM analysis

The QTAIM method was employed to investigate the intermolecular interactions between allicin and the nanocages (C_{24}, $B_{12}N_{12}$, and $Al_{12}N_{12}$) in the aqueous phase. This analysis provides essential information about the electron density (ρ), its Laplacian ($\nabla^2\rho$), total energy density (H(r)), potential energy density (V(r)), and kinetic energy density (G(r)) at bond critical points (BCPs), which helps in understanding the strength and nature of the interactions between allicin and the nanocages[38,39]. The QTAIM results are summarized in Table 2 and illustrated in Fig. 3.

For the interpretation of these parameters and to distinguish between weak and strong interactions, specific empirical boundaries are used. Van der Waals interactions typically have ρ values less than 0.005 a.u., a positive $\nabla^2\rho$, and G(r)/|V(r)| greater than 1.5. Hydrogen bonds are characterized by ρ values ranging from 0.01 to 0.04 a.u., a positive $\nabla^2\rho$, H(r) close to zero or positive, and G(r)/|V(r)| values between 1.0 and 1.2. Weak covalent interactions are usually observed with ρ values between 0.05 and 0.10 a.u., a negative $\nabla^2\rho$, and H(r) close to zero or negative, with G(r)/|V(r)| generally less than or near 1[38,39].

In the Allicin/C_{24} complex, several bond critical points were found between the carbon atoms of the C_{24} nanocage and the oxygen (O), sulfur (S), and hydrogen (H) atoms of allicin. The most prominent interaction occurred between the C atom of the nanocage and the O atom of allicin, with an electron density (ρ) of 0.22380 a.u. and a Laplacian of electron density ($\nabla^2\rho$) of 0.08876 a.u. The positive value of $\nabla^2\rho$ indicates a depletion of electron density at the BCP, characteristic of noncovalent interactions. Furthermore, the total energy density (H(r)) was positive (0.28835 a.u.), reinforcing the idea of a noncovalent interaction, potentially dative in nature. Other interactions, such as C…H and C…S, showed lower electron densities ($\rho < 0.01$ a.u.) and G(r)/|V(r)| ratios greater than 1.3, indicating that these interactions lie between weak hydrogen bonds and van der Waals forces, with van der Waals characteristics being more dominant.

In the Allicin/$B_{12}N_{12}$ complex, the QTAIM analysis revealed a significant interaction between the boron (B) atoms of the nanocage and the oxygen (O) atom of allicin. The electron density (ρ) at the B-O BCP was 0.13423 a.u., with a Laplacian of electron density ($\nabla^2\rho$) of −0.13441 a.u. and H(r) of 0.08212 a.u. The negative value of $\nabla^2\rho$ suggests a concentration of electron density at the BCP, indicative of covalent interactions. The ratio G(r)/|V(r)| = 0.70250 suggests a considerable ionic contribution, pointing to a partially covalent interaction with ionic character. Weaker interactions were also observed between the B atoms and the hydrogen (H) atoms of allicin, with $\rho \approx 0.01212$ a.u., which align with hydrogen bonding, as indicated by the G(r)/|V(r)| ratio greater than 1.

For the Allicin/$Al_{12}N_{12}$ complex, the QTAIM analysis revealed notable interactions between the aluminum (Al) atoms of the nanocage and the oxygen (O) atom of allicin. The electron density at the Al-O BCP was 0.06348 a.u., with a Laplacian of electron density ($\nabla^2\rho$) of −0.11532 a.u. and H(r) of −0.00750 a.u. The negative value of $\nabla^2\rho$ suggests a concentration of electron density at the BCP, indicating a covalent interaction. The ratio G(r)/|V(r)| of 1.07476 indicates a balance between kinetic and potential energy densities, suggesting a partially covalent interaction with ionic character. Additionally, interactions were observed between the nitrogen (N) atom of the nanocage and the hydrogen (H) atom of allicin, with $\rho \approx 0.01659$ a.u., which aligns with hydrogen bonding, as indicated by the G(r)/|V(r)| ratio greater than 1.

Complex	Bond	H(*r*)	$^2\nabla\rho$	ρ	G(*r*)	V(*r*)	Gr/|V|(*r*)
Allicin/C_{24}	C…..O	0.28835	0.08876	0.22380	0.49959	0.48794	1.02387
	C….H1	−0.00129	−0.00627	0.00759	0.00498	0.00368	1.35326
	C….S	−0.00089	−0.00563	0.00799	0.00474	0.00384	1.23437
	C….H2	−0.00082	−0.00379	0.00488	0.00297	0.00214	1.38785
Allicin/$B_{12}N_{12}$	B….O	0.08212	−0.13441	0.13423	0.21653	0.29865	0.70250
	B….H1	−0.00081	−0.00891	0.01212	0.00811	0.00730	1.11096
	B….H2	−0.00085	−0.00344	0.00394	0.00259	0.00175	1.48000
Allicin/$A_{12}N_{12}$	Al….O	−0.00750	−0.11532	0.06348	0.10782	0.10032	1.07476
	N…..H	−0.00030	−0.01119	0.01659	0.01088	0.01058	1.02835

Table 2. QTAIM analysis of Allicin/C_{24}, allicin/$b_{12}n_{12}$, and allicin/$al_{12}n_{12}$ complexes in the water phase at bond critical points (BCPs); data values are given in atomic units (a.u.).

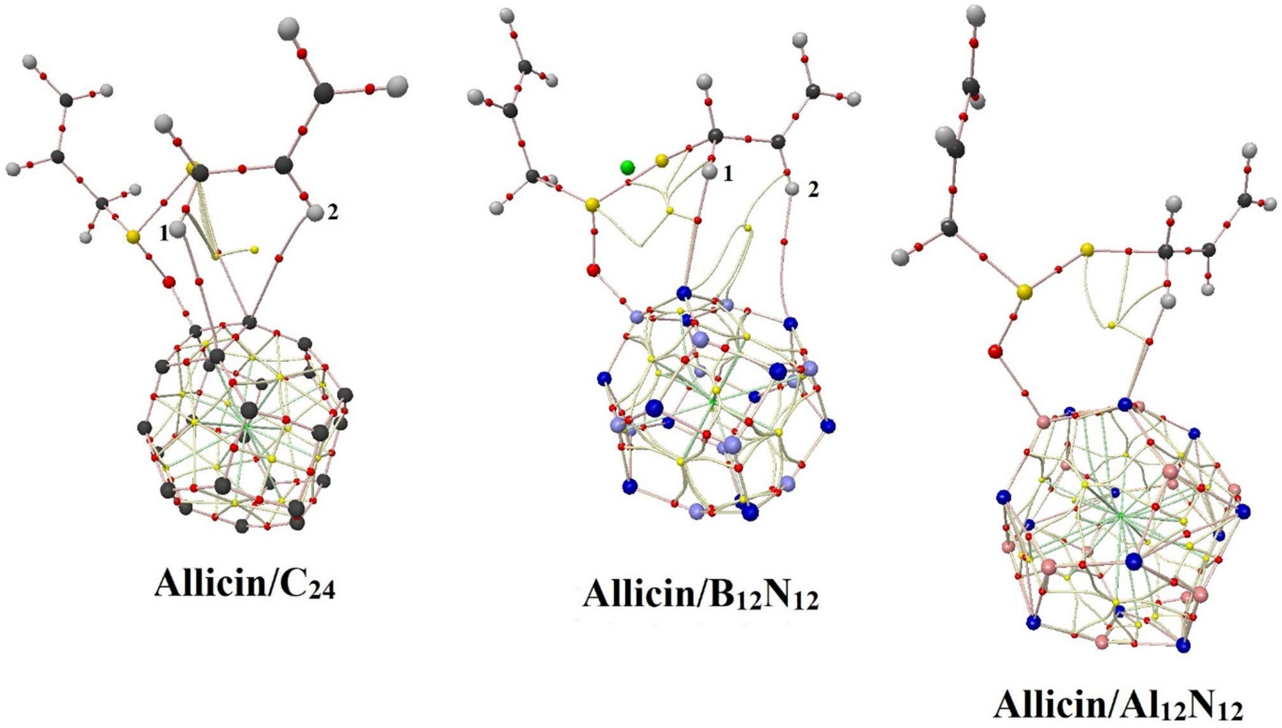

Allicin/C_{24} Allicin/$B_{12}N_{12}$ Allicin/$Al_{12}N_{12}$

Fig. 3. QTAIM analysis allicin/C_{24}, allicin/$B_{12}N_{12}$, and allicin/$Al_{12}N_{12}$ complexes in the water phase.

In summary, the interactions in the three complexes can be categorized as follows: The Allicin/C_{24} complex features very weak noncovalent interactions, including van der Waals and weak hydrogen bonds. The Allicin/$B_{12}N_{12}$ complex exhibits weak covalent interactions with notable ionic character, while the Allicin/$Al_{12}N_{12}$ complex displays relatively stronger covalent interactions with significant electron density sharing. This detailed analysis addresses the request to clarify the distinction between hydrogen bonding, van der Waals forces, and weak covalent interactions, providing a more precise understanding of the nature of the interactions in these complexes.

UV-Vis analysis

The UV-Vis absorption spectra of the allicin molecule and its complexes with C_{24}, $B_{12}N_{12}$, and $Al_{12}N_{12}$ nanocages were computed using the TD-DFT approach at the PBE1PBE-D3/6–31 +G** level of theory. The theoretical spectra for these systems in the aqueous phase are presented in Fig. 4, and the corresponding optoelectronic properties, including the excitation energy (E), maximum absorption wavelength (λmax), oscillator strength (f), and molar absorption coefficient (ε), are summarized in Table 3. The allicin molecule exhibited distinct absorption peaks in the range of 171.54–228.75 nm with oscillator strengths ranging from 0.1332 to 0.2001, indicating moderate absorption in the UV region. The corresponding molar extinction coefficients varied from 25123.2 $Lmol^{-1}\cdot cm^{-1}$ to 37202.2 $Lmol^{-1}\cdot cm^{-1}$, reflecting the molecule's inherent electronic transitions.

Upon complexation with nanocages, significant redshifts in λmax were observed, indicating strong interactions between allicin and the nanocages. For the Allicin/C_{24} complex, prominent peaks appeared at 248.70–312.20 nm, accompanied by an enhanced oscillator strength (up to 0.3504) and molar absorption coefficients reaching 70925.3 $Lmol^{-1}\cdot cm^{-1}$. Similarly, the Allicin/$B_{12}N_{12}$ and Allicin/$Al_{12}N_{12}$ complexes displayed maximum absorption wavelengths at 193.70–247.55 nm, with corresponding molar absorption coefficients as high as 104634.5 3 $Lmol^{-1}\cdot cm^{-1}$ for the Allicin/$Al_{12}N_{12}$ system. The observed redshifts and increased ε values for the complexes indicate enhanced electronic conjugation and stronger light absorption, which can be attributed to charge transfer between allicin and the nanocage surfaces. These findings suggest that the nanocages, significantly, modify the optoelectronic properties of allicin, making these complexes promising candidates for biomedical applications requiring enhanced UV-Vis activity.

Infrared spectroscopy

The vibrational characteristics of allicin and its complexes with nanocages (C_{24}, $B_{12}N_{12}$, and $Al_{12}N_{12}$) were analyzed using detailed infrared (IR) spectroscopy. The FTIR spectra of allicin and its complexes were determined in the aqueous phase to investigate the nature of bonds and interactions, with the results presented in Table 4; Fig. 5. Allicin exhibited characteristic peaks at 1065.53 cm-1 (strong, S = O stretching), 470.02 cm-1 (medium, S-S stretching), and 22.01 cm-1 (weak, S-S bending). These peaks indicate the presence of S = O and disulfide (S-S) bonds, which are crucial for allicin's structure and biological activity. For the Allicin/C24 complex, the S = O stretching vibration appeared at 772.48 cm-1, suggesting a shift due to interaction with the C24 nanocage. The S-S stretching vibration was observed at 505.51 cm-1, indicating a modification in the S-S

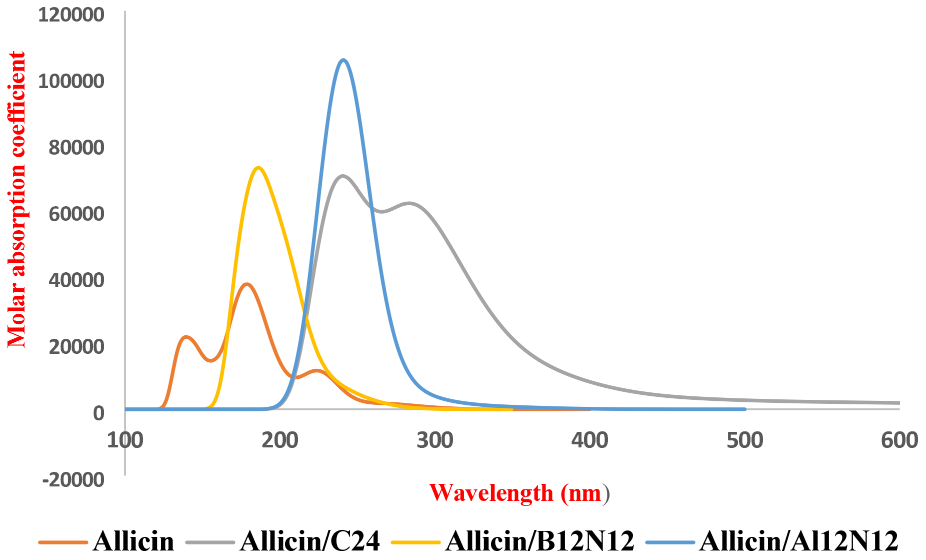

Fig. 4. Theoretical UV-Vis spectra computed for the allicin molecule and its complexes with C_{24}, $B_{12}N_{12}$, and $Al_{12}N_{12}$ in the water phase.

Compound	E/eV	λ_{max}/nm	f	ε
Allicin	6.78	182.90	0.2001	37202.2
	7.14	173.73	0.1594	30993.3
	7.23	171.54	0.1506	27856.4
	5.42	228.75	0.1393	25980.6
	6.58	188.53	0.1390	25789.5
	6.29	197.16	0.1332	25123.2
Allicin/C_{24}	4.44	279.41	0.3504	70925.3
	3.97	296.22	0.2137	43685.4
	4.99	248.70	0.2009	40905.2
	4.718	312.20	0.1982	40175.5
Allicin/$B_{12}N_{12}$	6.18	200.64	0.2519	72688.5
	6.40	193.70	0.2269	64908.9
Allicin/$Al_{12}N_{12}$	5.07	244.58	0.2736	104634.5
	5.02	247.55	0.1876	71758.9

Table 3. Optoelectronic properties of the allicin and its complexes with C_{24}, $B_{12}N_{12}$, and $Al_{12}N_{12}$ in the water phase.

bond upon complexation. A new strong peak at 935.97 cm-1 corresponds to O-C stretching, suggesting an interaction between allicin and the carbon atom of the C24 nanocage.

Similarly, in the Allicin/B12 N12 complex, the S = O stretching vibration is observed at 907.25 cm-1, similar to that observed for allicin, indicating that this bond remains largely intact. The S-S stretching vibration was observed at 491.48 cm-1, suggesting interaction with the B12 N12 nanocage. The strong peak at 917.77 cm-1 corresponds to O-B stretching, indicating bonding with boron atoms in the nanocage. For the Allicin/Al12 N12 complex, the S = O stretching vibration is observed at 935.02 cm-1, similar to that observed for allicin, indicating that this bond remains largely unaffected. The S-S stretching vibration was observed at 488.90 cm-1, suggesting interaction with the Al12 N12 nanocage. The strong peak at 586.82 cm-1 corresponds to O-Al stretching, suggesting interaction with aluminum atoms in the nanocage. These IR spectral changes provide evidence of the interaction between allicin and the nanocages, with new bonding interactions involving O-C, O-B, and O-Al bonds. The shifts in peak frequencies and the appearance of new peaks are consistent with the adsorption energy and electronic property data, further confirming the stability and nature of the allicin-nanocage complexes. These findings are crucial for understanding the structural modifications and potential therapeutic implications of allicin when complexed with these nanocages.

Compound	Peak No.	Frequency (cm^{-1})	Relative intensity	Vibration mode	Functional group	Remarks
Allicin	1	1065.53	Strong	Stretching (S = O)	Sulfoxide	Characteristic peak of the sulfoxide bond in allicin.
	2	470.02	Medium	Stretching (S-S)	Disulfide	The presence of disulfide bonds.
	3	22.01	Weak	Bending (S-S)	Disulfide	Weak bending vibration of the disulfide bond.
Allicin/C_{24}	1	772.48	Medium	Stretching (S = O)	Sulfoxide	Interaction with C24 affects the S = O vibration.
	2	505.51	Medium	Stretching (S-S)	Disulfide	Interaction with C24 modifies S-S vibration.
	3	935.97	Strong	Stretching (O-C)	Oxygen-Carbon	Interaction between oxygen in allicin and carbon in C_{24} nanocage.
Allicin/$B_{12}N_{12}$	1	907.25	Strong	Stretching (S = O)	Sulfoxide	Similar to allicin, indicating an S = O bond.
	2	491.48	Medium	Stretching (S-S)	Disulfide	Stretching vibrations indicate interactions with the nanocage.
	3	917.77	Strong	Stretching (O-B)	Oxygen-Boron	Interaction between oxygen in allicin and boron in $B_{12}N_{12}$ nanocage.
Allicin/$Al_{12}N_{12}$	1	935.02	Strong	Stretching (S = O)	Sulfoxide	Similar to allicin, indicating an S = O bond.
	2	488.90	Medium	Stretching (S-S)	Disulfide	Indicates bending vibrations in the modified environment.
	3	586.82	Strong	Stretching (O-Al)	Oxygen-Aluminum	Interaction between oxygen in allicin and aluminum in $Al_{12}N_{12}$ nanocage.

Table 4. Infrared spectroscopy data for allicin and its complexes in the water phase.

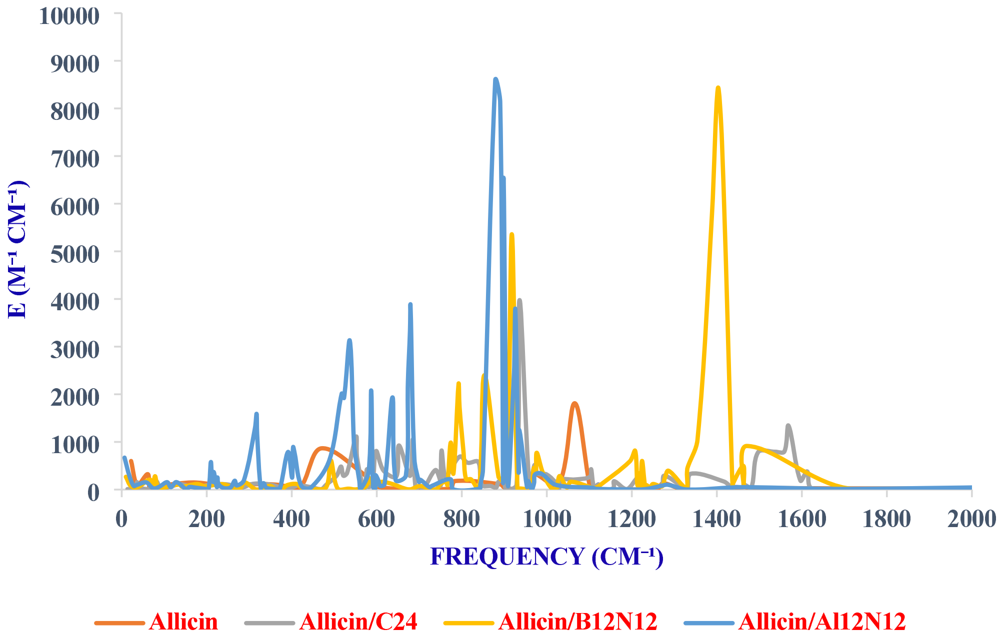

Fig. 5. FT-IR curves of the allicin molecule and its complexes with C_{24}, $B_{12}N_{12}$, and $Al_{12}N_{12}$ in the water phase.

Molecular docking analysis

The therapeutic potential of allicin and its complexes (Allicin/C_{24}, Allicin/$B_{12}N_{12}$, and Allicin/$Al_{12}N_{12}$) was evaluated through molecular docking analysis targeting key proteins involved in cancer (HER2), inflammation (TNF-α), COVID-19 (main protease), and bacterial infections (Staphylococcus aureus). The molecular docking results are summarized in Table 5, which provides detailed information on the binding affinity (E_{Dc}), inhibition constants (K_i), and interaction types (conventional hydrogen bonds, non-conventional hydrogen bonds, electrostatic interactions, and hydrophobic interactions) for allicin and its complexes with the target proteins. Additionally, Fig. 6 presents a 2D view of the intermolecular interactions between the studied compounds and the active sites of the proteins. These visual representations provide further insights into the binding mechanisms and interaction sites of ligands with target proteins. The results were compared with those of free allicin to assess the enhancement of binding affinity and interaction mechanisms. Lower K_i values indicate stronger binding affinity, which is critical for effective therapeutic interventions[46].

free allicin exhibited a binding energy of −3.74 kcal/mol with a Ki of 1.81 μM, forming conventional hydrogen bonds with Ile136 and non-conventional hydrogen bonds with Glu135, suggesting moderate binding affinity with TNF-α, a key cytokine in inflammation. The Allicin/$Al_{12}N_{12}$ complex demonstrated stronger binding affinity (E_{Dc} = −4.48 kcal/mol, K_i = 1.54 μM), forming a conventional hydrogen bond with Ile136 and electrostatic

Target protein	PDB ID	Ligand	E_{Dc} (kcal/mol)	Ki (μM)	Conventional hydrogen bonds	Nonconventional hydrogen bonds	Electrostatic Interactions	Hydrophobic interactions	Grid box size (X, Y, Z)	Grid center (X, Y, Z)
NF-alpha	2 AZ5	Allicin	−3.74	1.81	Ile136	Glu135	Glu135	Pro139, Leu26, and Trp28 Trp28	60, 60, 60	−26.64, 65.94, 41.97
		Allicin/C_{24}	−3.34	19.15	-	-	-	Ile136, Ieu26, Pro139:Pro139		
		Allicin/$B_{12}N_{12}$	−1.03	944.49	Ile136,Leu26,Asn46	Leu26	Glu135	Pro139, Ile136		
		Allicin/$Al_{12}N_{12}$	−4.48	1.54	Ile136	-	Gln25	-		
HER2	3RCD	Allicin	−3.78	1.70	ASP863	-	ASP863	Leu785, MET774, Lys753, PHE864, Lys753,PHE864, ALA751		12.5, 3.0, 28.1
		Allicin/C_{24}	−5.42	578.25	Cys805, Phe1004	Gly804	Glu812,Asp808	Leu 726, Cys 805, His 809Leu726, Cys805, His809		
		Allicin/$B_{12}N_{12}$	−2.49	80.65	Lys753	-	-	Leu852, Val734, Cys805, Arg849, Ala751, Leu800, Arg849,Ala751,Leu800, Leu796, Met801		
		Allicin/$Al_{12}N_{12}$	−7.21	27.98	Lys753	-	-	Leu852, Ala751, and Leu800Leu800		
COVID-19	6LU7	Allicin	−3.79	1.68	TYR54	ASP187	HIS164	Met49, Cys44, Pro52, and Met165, Pro52,Met165		−11.8, 13.2, 67.4
		Allicin/C_{24}	−5.59	435.04	Glu166	-	-	His41, Cys145, His163, Met49, and Met165Met165		
		Allicin/$B_{12}N_{12}$	−2.79	48.46	-	Gly143	His41,Cys145, Met49	Cys145, Met165		
		Allicin/$Al_{12}N_{12}$	−6.74	61.62	His41, Gly143, Cys145	Thr25	-	His41, His163, Cys145, Met49		
Staphylococcus aureus	3 VSL	Allicin	−4.15	907.75	Thr635,Gly620, Thr619	Tyr636	Tyr636	Val606, Pro660, Leu663, and Val658 Val658		18.3, −48.8, 23.3
		Allicin/C_{24}	−4.83	1.55	-	-	Glu623	Val632, Pro659, Pro661, Pro660, and Pro630Pro630		
		Allicin/$B_{12}N_{12}$	−1.86	235.96	-	-	Thr619	Pro661, Thr603,Tyr636		
		Allicin/$Al_{12}N_{12}$	−7.21	28.00	-	-	-	Tyr636		

Table 5. Molecular Docking analysis of allicin and its complexes (C_{24}, $B_{12}N_{12}$, $Al_{12}N_{12}$) on key therapeutic targets: TNF-alpha, HER2, COVID-19, and Staphylococcus aureus.

interactions with Gln25, indicating its potential as a highly effective TNF-α inhibitor. The Allicin/C_{24} complex showed moderate binding affinity (E_{Dc}= −3.34 kcal/mol, K_i= 19.15 μM), with hydrophobic interactions involving Ile136, Leu26, and Pro139, but its higher Ki value indicates weaker binding affinity compared with free allicin, making it less effective for inflammation therapy. The Allicin/$B_{12}N_{12}$ complex exhibited the weakest binding affinity (E_{Dc}= −1.03 kcal/mol, K_i= 944.49 μM), forming conventional hydrogen bonds with Ile136, Leu26, and Asn46, making it the least effective for inflammation therapy.

In the context of cancer therapy, free allicin exhibited a binding affinity of −3.78 kcal/mol with a Ki of 1.70 μM, forming conventional hydrogen bonds with ASP863 and hydrophobic interactions with Leu785 and MET774, suggesting moderate binding affinity with HER2, a key target in breast cancer therapy. In contrast, the Allicin/$Al_{12}N_{12}$ complex demonstrated significantly stronger binding affinity (E_{Dc}= −7.21 kcal/mol, Ki = 27.98 μM), forming conventional hydrogen bonds with Lys753 and hydrophobic interactions with Leu852 and Ala751, indicating its potential as a highly effective HER2 inhibitor. While the Allicin/C_{24} complex showed improved binding affinity (E_{Dc}= −5.42 kcal/mol, K_i = 578.25 μM) compared with free allicin, forming conventional hydrogen bonds with Cys805 and Phe1004, its high K_i value indicates weaker binding affinity, making it less suitable for HER2-targeted cancer therapy. The Allicin/$B_{12}N_{12}$ complex exhibited weaker binding affinity (E_{Dc}= −2.49 kcal/mol, Ki = 80.65 μM), forming only a single conventional hydrogen bond with Lys753, making it the least favorable for cancer therapy.

For COVID-19 therapy, free allicin exhibited a binding energy of −3.79 kcal/mol with a K_i of 1.68 μM, forming conventional hydrogen bonds with TYR54 and non-conventional hydrogen bonds with ASP187, suggesting moderate binding affinity with the COVID-19 main protease. The Allicin/$Al_{12}N_{12}$ complex demonstrated significantly stronger binding affinity (E_{Dc}= −6.74 kcal/mol, K_i= 61.62 μM), forming conventional hydrogen bonds with His41, Gly143, and Cys145, indicating its potential as a highly effective antiviral agent. The Allicin/

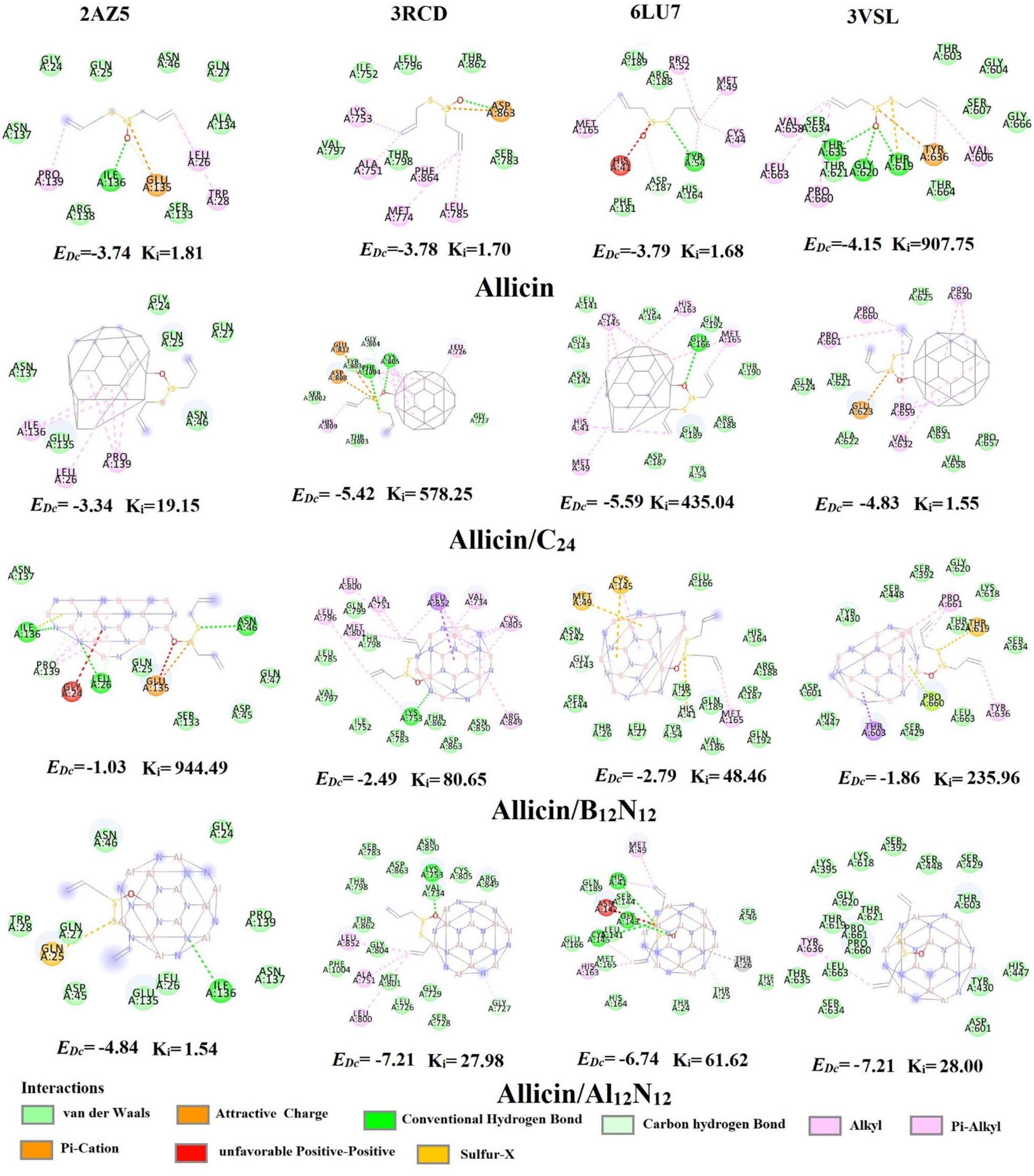

Fig. 6. 2D view of intermolecular interactions between allicin, allicin/C_{24}, allicin/$B_{12}N_{12}$, and allicin/$Al_{12}N_{12}$ compounds with the active sites of TNF-alpha (2 AZ5), HER2 (3RCD), COVID-19 (6LU7), and Staphylococcus aureus (3 VSL) proteins.

C_{24} complex showed strong binding affinity (E_{Dc}= −5.59 kcal/mol, K_i= 435.04 µM), forming a conventional hydrogen bond with Glu166, but its high Ki value indicates weaker binding affinity compared with free allicin, making it less effective for COVID-19 therapy. The Allicin/$B_{12}N_{12}$ complex exhibited weaker binding affinity (E_{Dc}= −2.79 kcal/mol, K_i= 48.46 µM), forming nonconventional hydrogen bonds with Gly143, making it the least effective for COVID-19 therapy.

In bacterial therapy, free allicin exhibited a binding energy of −4.15 kcal/mol with a K_i of 907.75 µM, forming conventional hydrogen bonds with Thr635, Gly620, and Thr619, suggesting moderate binding affinity with

Staphylococcus aureus. The Allicin/$Al_{12}N_{12}$ complex demonstrated significantly stronger binding affinity (E_{Dc}= −7.21 kcal/mol, K_i = 28.00 μM), forming hydrophobic interactions with Tyr636, indicating its potential as a highly effective antibacterial agent. The Allicin/C_{24} complex showed strong binding affinity (E_{Dc}= −4.83 kcal/mol, K_i= 1.55 μM), forming electrostatic interactions with Glu623, but its high K_i value indicates weaker binding affinity compared to free allicin, making it less effective for antibacterial therapy. The Allicin/$B_{12}N_{12}$ complex exhibited weaker binding affinity (E_{Dc}= −1.86 kcal/mol, K_i= 235.96 μM), forming electrostatic interactions with Thr619, making it the least effective antibacterial agent.

Overall, free allicin demonstrated moderate binding affinity across all therapeutic targets, making it a viable option for cancer, inflammation, COVID-19, and bacterial therapies. However, its binding affinities were generally weaker than those of the Allicin/$Al_{12}N_{12}$ complex, which consistently demonstrated the strongest binding affinities across all therapeutic targets, outperforming free allicin. The Allicin/C_{24} complex showed improved binding affinity compared to free allicin in some cases, but this was limited by its higher Ki values, which indicate weaker binding affinity. The Allicin/$B_{12}N_{12}$ complex exhibited weaker binding affinity and higher Ki values than free allicin, indicating its poor efficacy for therapeutic applications. The Allicin/$Al_{12}N_{12}$ complex is the most effective combination for cancer, inflammation, COVID-19, and bacterial therapies, outperforming free allicin. The Allicin/C_{24} complex shows potential but is less effective because of its higher Ki values. The Allicin/$B_{12}N_{12}$ complex is the least effective for therapeutic applications. Although no statistical test was conducted, the difference in binding affinities between free allicin and its complexes is considered sufficient to suggest a potentially meaningful enhancement in binding strength and biological interaction. Further experimental studies are required to validate these findings and optimize the therapeutic potential of these complexes.

Although molecular docking provides valuable preliminary insights into binding affinity and potential interaction modes between ligands and biological targets, it does not encompass the full complexity of pharmacological activity in vivo. In particular, parameters such as absorption, distribution, metabolism, excretion, and toxicity (ADMET) critically influence the therapeutic efficacy and safety of a drug candidate. Therefore, the docking results presented here should be interpreted with caution and viewed as a first step in drug discovery that necessitates subsequent validation through ADMET modeling and experimental studies[47,48].

A clear correlation was observed between the calculated electronic properties (HOMO-LUMO gap and quantum molecular descriptors (QMDs) and the binding affinities obtained from molecular docking studies. Generally, a reduction in the HOMO-LUMO gap upon complexation with nanocages correlates with increased chemical reactivity and stronger binding affinity toward biological targets such as HER2, TNF-α, SARS-CoV-2 Mpro, and Staphylococcus aureus. For instance, the Allicin/C_{24} complex, which exhibited the lowest energy gap (2.16 eV), showed enhanced electronic reactivity compared to free allicin. However, the Allicin/$Al_{12}N_{12}$ complex, despite having a higher energy gap (3.44 eV), demonstrated the strongest binding affinities across all targets. This could be attributed to its greater thermodynamic stability, favorable charge redistribution, and stronger non-covalent interactions such as hydrogen bonding and van der Waals forces. These findings suggest that while the HOMO-LUMO gap is a key indicator of electronic reactivity, other QMDs such as global hardness (η), chemical potential (μ), and electrophilicity index (ω) also significantly contribute to the binding behavior and biological activity. The integration of these descriptors enables a more comprehensive understanding of the structure activity relationship (SAR) for the designed complexes.

Conclusion

In this study, we conducted a comprehensive computational analysis of the anti-inflammatory, anticancer, antiviral, and antibacterial properties of allicin and its complexes with nanocages (Allicin/C_{24}, Allicin/$B_{12}N_{12}$, and Allicin/$Al_{12}N_{12}$) using advanced techniques such as Density Functional Theory (DFT), Quantum Theory of Atoms in Molecules (QTAIM), and molecular docking. The results demonstrated that allicin, a bioactive compound derived from garlic (Allium sativum), exhibits significant therapeutic potential, which can be further enhanced through its interaction with nanocages. The adsorption energy calculations revealed that allicin forms stable complexes with C_{24}, $B_{12}N_{12}$, and $Al_{12}N_{12}$ nanocages, with $Al_{12}N_{12}$ showing the strongest adsorption affinity in both gas and aqueous phases. However, the Gibbs free energy change (ΔG) for the Allicin/C_{24} complex was found to be positive ($\Delta G = 9.12$ kcal/mol in the gas phase), indicating a less thermodynamically favorable adsorption process compared to the other nanocages. In contrast, the Allicin/$B_{12}N_{12}$ and Allicin/$Al_{12}N_{12}$ complexes exhibited negative ΔG values, confirming their spontaneous and exothermic nature. These findings suggest that while C_{24} can still interact with allicin, its thermodynamic profile makes it less suitable for drug delivery applications compared to $B_{12}N_{12}$ and $Al_{12}N_{12}$.

QTAIM analysis provided detailed insights into the nature of the interactions, revealing a combination of noncovalent (e.g., hydrogen bonding and van der Waals forces) and partially covalent interactions, depending on the nanocage type. These findings highlight the potential of nanocages to improve the stability and bioavailability of allicin. Molecular docking simulations further validated the therapeutic potential of allicin and its complexes. The Allicin/$Al_{12}N_{12}$ complex exhibited the highest binding affinity with key biological targets, including HER2 (a cancer target), TNF-α (an inflammation mediator), COVID-19 main protease, and Staphylococcus aureus (a bacterial pathogen). This suggests that the Allicin/$Al_{12}N_{12}$ complex could serve as a potent candidate for cancer therapy, anti-inflammatory therapy, antiviral therapy, and antibacterial intervention. The Allicin/C_{24} and Allicin/$B_{12}N_{12}$ complexes also showed promising results although their binding affinities were generally weaker than those of Allicin/$Al_{12}N_{12}$.

Spectroscopic analyses, including UV-Vis and IR spectroscopy, provided additional evidence of the enhanced electronic and structural properties of allicin upon complexation with nanocages. Significant redshifts in the UV-Vis spectra and shifts in vibrational frequencies in the IR spectra confirmed the strong interactions between allicin and the nanocages, as well as the potential for improved drug delivery and therapeutic efficacy. In summary, this study highlights the significant potential of allicin-nanocage complexes, particularly Allicin/

$Al_{12}N_{12}$, as novel therapeutic agents for a wide range of diseases, including cancer, inflammation, viral infections, and bacterial infections. The integration of computational methods such as DFT, QTAIM, and molecular docking has provided valuable insights into the molecular interactions and mechanisms underlying the pharmacological effects of these complexes. These findings not only underscore the importance of natural products in drug discovery and demonstrate the critical role of computational approaches in optimizing drug design and development. Future experimental studies are needed to validate these computational predictions and further explore the therapeutic applications of allicin-nanocage complexes.

Data availability

The research described in this article did not use any data.

Received: 25 March 2025; Accepted: 20 May 2025

References

1. Cavallito, C. J. & Bailey, J. H. Allicin, the antibacterial principle of Allium sativum. I. Isolation, physical properties and antibacterial action. *J. Am. Chem. Soc.* **66** (11), 1950–1951. https://doi.org/10.1021/ja01239a048 (1944).
2. Savairam, V. D., Patil, N. A., Borate, S. R., Ghaisas, M. M. & Shete, R. V. Allicin: A review of its important Pharmacological activities. *Pharmacol. Res. - Mod. Chin. Med.* **8**, 100283. https://doi.org/10.1016/j.prmcm.2023.100283 (2023).
3. Dhakar, S., Tare, H. & Jain, S. K. Exploring the therapeutic potential of Allium sativum: recent advances and applications. *Int. J. Pharm. Qual. Assur.* **14** (04), 1283–1286. https://doi.org/10.25258/ijpqa.14.4.70 (2023).
4. Li, X. et al. Allicin inhibits the growth of HONE-1 and HNE1 human nasopharyngeal carcinoma cells by inducing ferroptosis. *Neoplasma* **71** (03), 243–254. https://doi.org/10.4149/neo_2024_240108n8 (2024).
5. Catanzaro, E., Canistro, D., Pellicioni, V., Vivarelli, F. & Fimognari, C. Anticancer potential of allicin: A review. *Pharmacol. Res.* **177**, 106118. https://doi.org/10.1016/j.phrs.2022.106118 (2022).
6. Choo, S. et al. Review: antimicrobial properties of allicin used alone or in combination with other medications. *Folia Microbiol.* **65** (3), 451–465. https://doi.org/10.1007/s12223-020-00786-5 (2020).
7. Marchese, A. et al. Antifungal and antibacterial activities of allicin: A review. *Trends Food Sci. Technol.* **52**, 49–56. https://doi.org/10.1016/j.tifs.2016.03.010 (2016).
8. Mousa, A. M. et al. Could allicin alleviate trastuzumab-induced cardiotoxicity in a rat model through antioxidant, anti-inflammatory, and antihyperlipidemic properties? *Life Sci.* **302**, 120656. https://doi.org/10.1016/j.lfs.2022.120656 (2022).
9. Swarna, M. R. et al. Understanding the adsorption performance of hetero-nanocages (C12–B6N6, C12–Al6N6, and B6N6–Al6N6) towards hydroxyurea anticancer drug: a comprehensive study using DFT. *Nanoscale Adv.* https://doi.org/10.1039/d4na00472h (2024).
10. Fouegue, A. D. T. et al. DFT investigation of Temozolomide drug delivery by pure and Boron doped C24fullerene-like nanocages. *Nanoscale Adv.* **5** (21), 5880–5891. https://doi.org/10.1039/d3na00402c (2023).
11. Nair, R. G. S., Nair, A. K. N. & Sun, S. Adsorption of drugs on B12N12 and Al12N12 nanocages. *RSC Adv.* **14** (43), 31756–31767. https://doi.org/10.1039/d4ra05586a (2024).
12. Wu, S. et al. Investigating the drug carrying ability of al and Ga doped B12N12 nanocages for 5-fluorouracil based on DFT. *New J. Chem.* **47** (24), 11478–11491. https://doi.org/10.1039/d3nj00947e (2023).
13. Padash, R. et al. Is it possible to use X12Y12 (X = Al, B, and Y = N, P) nanocages for drug-delivery systems? A DFT study on the adsorption property of 4-aminopyridine drug. *Appl. Phys. A.* **124** (9). https://doi.org/10.1007/s00339-018-1965-y (2018).
14. Safa, A. N., Sheibani, A., Baei, M. T., Sayyed-Alangi, S. Z. & Lemeski, E. T. Theoretical and experimental studies on sulfasalazine interactions with Poly (lactic acid): impact of hydrogen bonding and charge transfer interactions on molecular structure, electronic and optical properties. *Heliyon* **10** (1), e23813. https://doi.org/10.1016/j.heliyon.2023.e23813 (2023).
15. Safa, A. N., Sheibani, A., Baei, M. T., Sayyed-Alangi, S. Z. & Lemeski, E. T. OLEIC ACID AS AN EFFECTIVE SURFACTANT FOR POLY (LACTIC ACID) MICROPARTICLE: a DFT STUDY. *Izv. Vyssh. Uchebn. ZAVEDENIY Khim. KHIMICHESKAYA Tekhnol.* **67** (6), 65–72. https://doi.org/10.6060/ivkkt.20246706.7069 (2024).
16. Doust Mohammadi, M. & Hamzehloo, M. The adsorption of bromomethane onto the exterior surface of aluminum nitride, Boron nitride, carbon, and silicon carbide nanotubes: A PBC-DFT, NBO, and QTAIM study. *Comput. Theor. Chem.* **1144**, 26–37. https://doi.org/10.1016/j.comptc.2018.10.001 (2018).
17. Doust Mohammadi, M. & Abdullah, H. Y. The adsorption of Bromochlorodifluoromethane on pristine, al, Ga, P, and As-doped Boron nitride nanotubes: A study involving PBC-DFT, NBO analysis, and QTAIM. Computational and Theoretical Chemistry, **1193**, 113047. (2021). https://doi.org/10.1016/j.comptc.2020.113047
18. Doust Mohammadi, M. & Abdullah, H. Y. The adsorption of chlorofluoromethane on pristine, Al-, Ga-, P-, and As-doped Boron nitride nanotubes: A PBC-DFT, NBO, and QTAIM study. *ChemistrySelect* **5** (39), 12115–12124. https://doi.org/10.1002/slct.202003367 (2020).
19. Doust Mohammadi, M. et al. Advancing optoelectronic performance of organic solar cells: computational modeling of non-fullerene donor based on end-capped Triphenyldiamine (TPDA) molecules. *Comput. Theor. Chem.* **1226**, 114201. https://doi.org/10.1016/j.comptc.2023.114201 (2023).
20. Doust Mohammadi, M., Abdullah, H. Y., Louis, H., Etim, E. E. & Edet, H. O. Evaluating the detection potential of C59X fullerenes (X = C, Si, Ge, B, al, Ga, N, P, and As) for H2SiCl2 molecule. *J. Mol. Liq.* **387**, 122621. https://doi.org/10.1016/j.molliq.2023.122621 (2023).
21. Mohammadi, M. D. et al. Hexachlorobenzene (HCB) adsorption onto the surfaces of C60, C59Si, and C59Ge: insight from DFT, QTAIM, and NCI. *Chem. Phys. Impact*. **6**, 100234. https://doi.org/10.1016/j.chphi.2023.100234 (2023).
22. Mohammad, M. D., Abbas, F., Louis, H. & Amodu, I. O. Halides (Cl, F, and Br) encapsulated Ga12As12 nanocages used to improve the cell voltage for enhanced battery performance. *J. Phys. Chem. Solids.* **174**, 111174. https://doi.org/10.1016/j.jpcs.2022.111174 (2023).
23. Doust Mohammadi, M., Abdullah, H. Y., Qadir, K. W. & Suvitha, A. Theoretical investigation of intermolecular interactions between CNT, SiCNT and sicgent nanomaterials with vinyl chloride molecule: A DFT, NBO, NCI, and QTAIM study. *Diam. Relat. Mater.* **131**, 109602. https://doi.org/10.1016/j.diamond.2022.109602 (2023).
24. Doust Mohammadi, M., Abdullah, H. Y., Biskos, G. & Bhowmick, S. Adsorbing CNCl on pristine, C-, and Al-doped Boron nitride nanotubes: A density functional theory study. *Comput. Theor. Chem.* **1220**, 113980. https://doi.org/10.1016/j.comptc.2022.113980 (2023).
25. Soltani, A., Azmoodeh, Z., Bezi Javan, M., Tazikeh Lemeski, E. & Karami, L. A DFT study of adsorption of glycine onto the surface of BC_2N nanotube. *Appl. Surf. Sci.* **384**, 230–236. https://doi.org/10.1016/j.apsusc.2016.04.162 (2016).

26. Soltani, A., Ramezani Taghartapeh, M., Tazikeh Lemeski, E., Abroudi, M. & Mighani, H. A theoretical study of the adsorption behavior of N2O on single-walled AlN and alp nanotubes. *Superlattices Microstruct.* **58**, 178–190. https://doi.org/10.1016/j.spmi.2013.02.015 (2013).
27. Doust Mohammadi, M. et al. Gas-Phase Interaction of CO, H2S, NH3, NO, NO2, and SO2 with Zn12O12 and Zn24 Atomic Clusters. ACS Omega, 8 (23), 20621–20633. (2023). https://doi.org/10.1021/acsomega.3c01177
28. Ernzerhof, M. & Scuseria, G. E. Assessment of the Perdew-Burke-Ernzerhof exchange correlation functional. *J. Chem. Phys.* **110**, 5029e36 (1999).
29. Becke, A. D. & Johnson, E. R. A density-functional model of the dispersion interaction. *J. Chem. Phys.* **123**, 154101. https://doi.org/10.1063/1.2065267 (2005).
30. 01, D. et al. (2009). J.V. Ortiz, J. Cioslowski, D.J. Fox, Gaussian 09, Revision, Gaussian, Inc., Wallingford CT.
31. Latypov, S. K., Polyancev, F. M., Yakhvarov, D. G. & Sinyashin, O. G. Quantum chemical calculations of ^{31}P NMR chemical shifts: scopes and limitations. *Phys. Chem. Chem. Phys.* **17** (11), 6976–6987. https://doi.org/10.1039/C5CP00240K (2015).
32. Grimme, S., Antony, J., Ehrlich, S. & Krieg, H. A consistent and accurate Ab initio parametrization of density functional dispersion correction (DFT-D) for the 94 elements H-Pu. *J. Chem. Phys.* **132**, 154104. https://doi.org/10.1063/1.3382344 (2010).
33. Goerigk, L. & Grimme, S. A thorough benchmark of density functional methods for general main group thermochemistry, kinetics, and noncovalent interactions. *Phys. Chem. Chem. Phys.* **13**, 6670–6688. https://doi.org/10.1039/C0CP02984J (2011).
34. Li, X. et al. Hydrogen bond and π-π stacking interaction: stabilization mechanism of two metal Cyclo-N5−-Containing energetic materials. *ACS Omega*. **7** (8), 6627–6639. https://doi.org/10.1021/acsomega.1c05961 (2022).
35. Derakhshandeh, M. & Anaraki-Ardakani, H. A computational study on the experimentally observed sensitivity of Ga-doped ZnO nanocluster toward CO gas. *Phys. E: Low-dimensional Syst. Nanostruct.* **84**, 298–302. https://doi.org/10.1016/j.physe.2016.06.026 (2016).
36. Boys, S. F. & Bernardi, F. The calculation of small molecular interactions by the differences of separate total energies. Some procedures with reduced errors. *Mol. Phys.* **19** (4), 553–566 (1970).
37. Karelson, M., Lobanov, V. S. & Katritzky, A. R. Quantum-chemical descriptors in QSAR/QSPR studies. *Chem. Rev.* **96** (3), 1027–1044. https://doi.org/10.1021/cr950202r (1996).
38. Bader, R. F. W. Atoms in molecules. *Acc. Chem. Res.* **18** (1), 9–15 (1985).
39. Bader, R. F. W. A quantum theory of molecular structure and its applications. *Chem. Rev.* **91** (5), 893–928 (1991).
40. Marenich, A. V., Cramer, C. J. & Truhlar, D. G. Universal solvation model based on solute electron density and on a continuum model of the solvent defined by the bulk dielectric constant and atomic surface tensions. *J. Phys. Chem. B.* **113** (18), 6378–6396. https://doi.org/10.1021/jp810292n (2009).
41. Morris, G. M. et al. Olson, AutoDock4 and AutoDockTools4: automated Docking with selective receptor flexibility. *J. Comput. Chem.* **30** (16), 2785–2791 (2009).
42. Fouegue, A. D. T. et al. DFT investigation of Temozolomide drug delivery by pure and Boron doped C24fullerene-like nanocages. *Nanoscale Adv.* **5** (21), 5880–5891. https://doi.org/10.1039/d3na00402c (2023b).
43. Saadh, M. J. et al. Inhibitory effects of menthol, B12N12, B16N16, Al12N12, Al16N16, and their complexes on tumor necrosis factor-alpha (TNF-α) and their potential anti-inflammatory activity: A study using DFT and molecular Docking. *Inorg. Chem. Commun.* **162**, 112187. https://doi.org/10.1016/j.inoche.2024.112187 (2024).
44. Rad, A. S. & Ayub, K. J. A comparative density functional theory study of guanine chemisorption on Al12N12, Al12P12, B12N12, and B12P12nano–cages. *J. Alloys Compd.* **672**, 161–169 (2016).
45. Ogunwale, G. J. et al. Interaction of 5-Fluorouracil on the surfaces of pristine and functionalized Ca12O12 nanocages: an intuition from DFT. *ACS Omega*. **8** (15), 13551–13568. https://doi.org/10.1021/acsomega.2c03635 (2023).
46. Irwin, J. J. et al. Automated Docking screens: a feasibility study. *J. Med. Chem. 52 (Sep.* **(18)**, 5712–5720. https://doi.org/10.1021/jm9006966 (2009).
47. Van de Waterbeemd, H. & Gifford, E. ADMET in Silico modelling: towards prediction Paradise?? *Nat. Rev. Drug Discovery*. **2** (3), 192–204. https://doi.org/10.1038/nrd1032 (2003).
48. Kitchen, D. B., Decornez, H., Furr, J. R. & Bajorath, J. Docking and scoring in virtual screening for drug discovery: methods and applications. *Nat. Rev. Drug Discovery*. **3** (11), 935–949. https://doi.org/10.1038/nrd1549 (2004).

Acknowledgements

The authors express their sincere gratitude to the Islamic Azad University, Gorgan Branch, for their invaluable support and resources.

Author contributions

E.S. Mozafari: Methodology, Data curation, Formal analysis, Writing – original draft.Mohammad T. Baei: Supervision, Project administration, Conceptualization, Validation, Writing – review & editing.E. Tazikeh Lemeski: Investigation, Software, Visualization, Writing – review & editing.

Declarations

Competing interests

The authors declare no competing interests.

Additional information

Correspondence and requests for materials should be addressed to M.T.B.